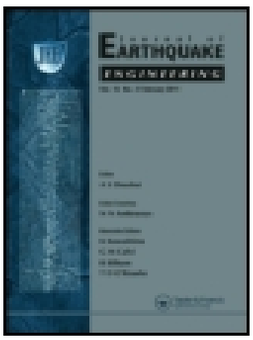

Journal of Earthquake Engineering

ISSN: 1363-2469 (Print) 1559-808X (Online) Journal homepage: http://www.tandfonline.com/loi/ueqe20

Parameters Affecting Dynamics of Three-Dimensional Seismic Isolation

Walaa Eltahawy, Keri L. Ryan, Sevki Cesmeci & Faramarz Gordaninejad

To cite this article: Walaa Eltahawy, Keri L. Ryan, Sevki Cesmeci & Faramarz Gordaninejad (2018): Parameters Affecting Dynamics of Three-Dimensional Seismic Isolation, Journal of Earthquake Engineering, DOI: 10.1080/13632469.2018.1537902

To link to this article: https://doi.org/10.1080/13632469.2018.1537902

Published online: 16 Nov 2018.

JOURNAL OF EARTHQUAKE ENGINEERING
https://doi.org/10.1080/13632469.2018.1537902

Parameters Affecting Dynamics of Three-Dimensional Seismic Isolation

Walaa Eltahawy[a], Keri L. Ryan[a], Sevki Cesmeci[b], and Faramarz Gordaninejad[b]

[a]Civil and Environmental Engineering, University of Nevada, Reno, 89557, USA; [b]Mechanical Engineering, University of Nevada, Reno, 89557, USA

ABSTRACT

Seismic base isolation systems are mainly used to reduce seismic demands and minimize earthquake effect on structure performance. In this study, the fundamental dynamic response of structures with three-dimensional (3D) isolation systems is explored using a simplified rigid block model. A parametric study is carried out to evaluate the effect of different site conditions, structure properties and 3D isolation parameters on structure and bearing response. The results show that the acceptable range of 3D isolation periods is 0.5–1.0 s for vertical direction with horizontal isolation period around 3–4 times the vertical period and 20% damping in both directions.

ARTICLE HISTORY
Received 17 April 2018
Accepted 9 October 2018

KEYWORDS
3D Isolation; Horizontal Excitation; Vertical Excitation; Dynamic Response; Rocking; Rigid Block

1. Introduction

Earthquake shaking is one of the most critical problems that affect different structures. Earthquakes induce much larger structure acceleration and forces more than those developed from the static load only; therefore, seismic isolation systems are used to mitigate this effect. Seismic isolation provides a flexible interface that uncouples the structure from the ground. Typically, flexible isolators attenuate accelerations and forces caused by the earthquake through a lengthening of the structure period. The increased displacement demands as a result of the period lengthening are accommodated by the isolation devices. Several studies have examined seismic reliability and life cycle cost analysis of base-isolated structures. These analysis results showed that seismic isolation systems generally provide significant improvements to overall system reliability [Alhan and Gavin, 2005; Chen *et al.*, 2007; Castaldo *et al.*, 2016] and reductions in life cycle costs [Terzic *et al.*, 2014; Terzic andMahin, 2017; Cutfield *et al.*, 2016; Castaldo *et al.*, 2016].

Traditional isolation systems control only the horizontal shaking and do nothing to mitigate vertical shaking. Recent studies illustrate that for seismic resiliency, vertical component of shaking needs to be considered as well as horizontal shaking, and vertical shaking greatly affects the performance of seismically isolated structures. Furukawa *et al.* conducted a full-scale shaking test of a four-story base-isolated reinforced concrete building. The test showed that vertical accelerations were significantly amplified relative to the ground in some cases in a building with rubber isolation bearings [Furukawa *et al.*, 2013]. Another full-scale shaking test of a five-story base-isolated steel moment frame building was conducted by Ryan *et al.* [2016]. Observed

CONTACT Walaa Eltahawy walaaeltahawy@nevada.unr.edu
Color versions of one or more of the figures in the article can be found online at www.tandfonline.com/ueqe.

damage was attributed entirely to large vertical input acceleration, because the horizontal structural acceleration was constrained to relatively low levels. Both tests clarified that non-structural components and contents are greatly affected by vertical excitation intensity.

Nowadays, three-dimensional (3D) isolation system has been used to fulfill nuclear facility design requirements. A 3D base isolation system can be achieved through specially designed 3D isolation devices or by combining vertical base isolation devices and horizontal base isolation devices in series [Inoue *et al.*, 2004]. Suhara *et al.* [2003, 2005] developed 3D isolation by combining laminated rubber bearings as horizontal isolators in series with rolling seal-type air springs as vertical isolators. The rolling seal-type air spring is a steel/concrete cylinder lowered into an air cavity and attached with a rolling rubber seal. The proposed device was examined for earthquake excitation, and it performed as designed. Kashiwazaki *et al.* developed and tested a hydraulic system used for vertical isolation, also connected in series with laminated rubber bearings. The hydraulic system consisted of load carrying hydraulic cylinders filled with nitrogen gas, to which fluctuating pressure could be transmitted by the attached accumulator units [Kashiwazaki *et al.*, 2003]. Kageyama *et al.* proposed a 3D isolation system consisting of cable-reinforced air springs. The 3D air spring was composed of an inner cylinder attached to the base and an outer cylinder attached to the structure separated by an air cavity bounded by a flexible rubber sheet [Kashiwazaki *et al.*, 2003 and 2004]. A shaking table test proved the feasibility of the developed system. Shimizu Corporation also developed commercial solution for 3D isolation [Takahashi *et al.*, 2008] [Suhara *et al.*, 2008]. The proposed 3D seismic isolation device consists of a laminated rubber bearing for horizontal isolation and multiple air springs for vertical isolation. A rocking suppression device with an oil damper is used to control rocking vibration. The proposed system has been implemented on a three-story apartment house building. The system is quite complicated and perhaps cost prohibitive for wider implementation.

Finally, some researchers have focused on 3D isolation for a special class of long-span articulated or hangar structures. Li *et al.* [2013] suggested a 3D isolation bearing composed of a frictional sliding device in the horizontal direction and helical springs or disk springs in the vertical direction. A long-span hangar structure with these bearings was simulated using multistory frame modeling. The hangar structure with 3D bearings achieved improved performance by effectively reducing the axial force and acceleration response, while the displacement of the bearing remained within its predetermined range. Xu *et al.* [2012a, 2012b] proposed a new multidimensional earthquake isolation and mitigation device for protecting long-span reticulated structures due to strong earthquake motions. The developed device consisted of a viscoelastic bearing and several viscoelastic dampers. The proposed device provided substantial energy dissipation as the force–displacement hysteretic loops were observed to be full smooth ellipses.

All previous studies focused on the development of vertical or 3D isolation devices or systems. The proposed systems have vertical isolation periods on the order of 1–2 s and generally utilize dampers (oil dampers or viscous wall dampers) and rocking suppression devices to control both vertical and rocking displacements. However, little work has been done to investigate the fundamental dynamics of 3D isolation systems to select target design parameters. Zhou *et al.* [2016] examined the dynamic performance of several vertical and 3D isolation systems for potential application to modern nuclear facilities. An isolation system with vertical period (T_V) = 0.33 s was found to be feasible for the studied nuclear power plant model and could effectively reduce the vertical in-structure responses. Also, Zhou concluded that the rocking effect was obvious when T_V increased to 1.0 s, and vertical bearing displacements

were at least as large as the horizontal displacements for T_V = 2.3 s. Finally, the authors [Eltahawy *et al.*, 2017] presented preliminary results on the fundamental dynamic response of structures with both horizontal and vertical isolations based on only three ground motions. This article is an extension of that work and includes multiple ground motion ensembles for statistical analysis, as well as variations in soil conditions, structure properties and isolation characteristics.

The objective of this study is to identify governing parameters of 3D isolation system that optimize the overall response of the structure, considering the tradeoffs between different displacements and accelerations. Parameters that define the 3D isolation system include horizontal isolation period T_H, vertical isolation period T_V, damping ratios ζ and bilinear stiffness. Other relevant variables include site parameters, target spectra and building height/width or aspect ratio h/b. These parameters are varied widely to identify the parameters of an effective isolation system to mitigate both horizontal and vertical effects. The structural response is simulated as a two-dimensional (2D) rigid block on flexible isolators subject to both horizontal and vertical input excitations.

2. Site Parameters and Target Spectra

A hypothetical site location and soil type were defined to obtain target spectra representing the seismic hazard in the horizontal and vertical directions. The selected site is located in Los Angeles area on soil class (D) with Mapped Risk-Targeted Maximum Considered Earthquake (MCE_R), 5% damped spectral acceleration of S_S = 2.11g at short periods and S_1 = 0.74g at 1.0 s period. MCE_R horizontal and vertical target spectra were developed for this site according to ASCE 7–16 [American Society of Civil Engineers (ASCE), 2016] and FEMA P-750 [National Earthquake Hazards Reduction Program (NEHRP), 2009], respectively. Equations to calculate spectra are illustrated in Fig. 1 for the horizontal direction and Fig. 2 for the vertical direction. In these equations, $S_{MS} = F_a S_S$ and $S_{M1} = F_v S_1$ where

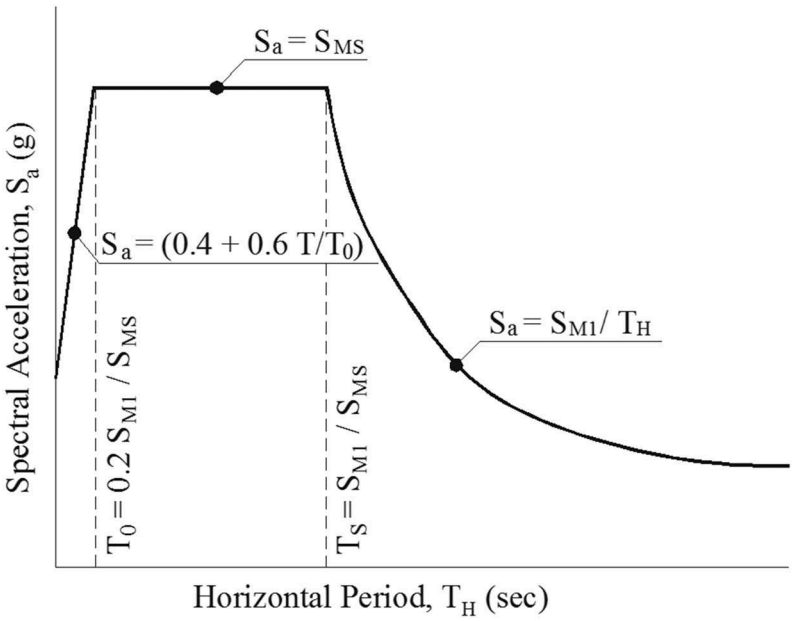

Figure 1. Horizontal MCE_R spectrum according to ASCE 7–16 [ASCE, 2016].

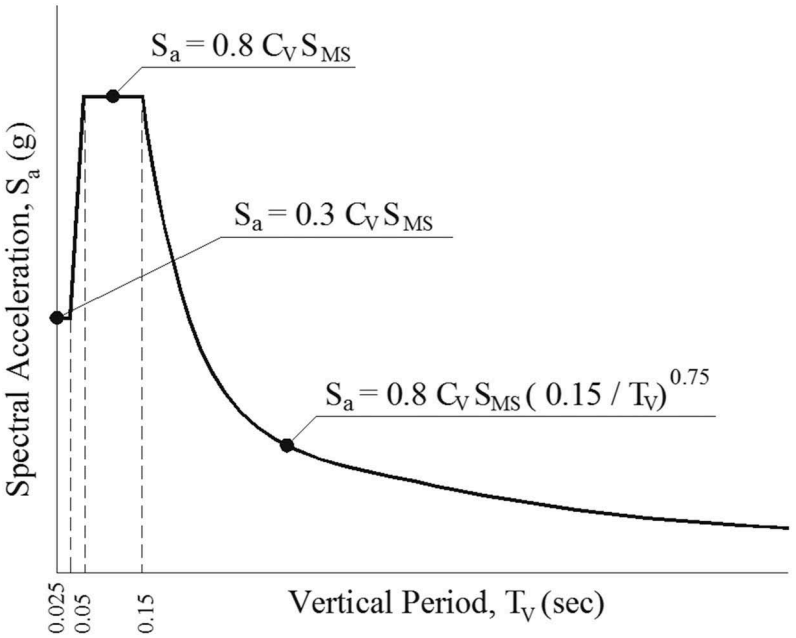

Figure 2. Vertical MCE_R spectrum according to FEMA P-750 [NEHRP, 2009].

F_a and F_v are site coefficients for short periods and 1.0 s periods, respectively. For site class (D) and $S_S \geq 1.25$g, $F_a = 1.0$, while $F_v = 1.5$ as $S_1 \geq 0.5$g. According to Section 23 of NEHRP [2009], C_V is a vertical coefficient that depends on S_S and site class. From Fig. 1 and 2, the peak vertical to horizontal spectral acceleration (V/H) ratio is observed to be $0.8C_V$. For site class (D), C_V varies from 0.7 for $S_S \leq 0.2$g to 1.5 for $S_S \geq 2.0$g; consequently, the V/H ratio ranges from 0.56 to 1.2. Based on S_S, the prescribed value is $V/H = 1.2$ for the given site. In addition, $V/H = 1.0$ and 0.75 were considered by modifying the target vertical spectra for the same horizontal spectra, to capture a wider range of ground motions and site conditions.

The developed horizontal and vertical MCE_R spectra with 5% damping and various V/H ratio are presented in Fig. 3. At longer periods, the vertical spectra are controlled by the requirement that vertical spectral acceleration does not fall below ½ of the horizontal spectral acceleration [NEHRP, 2009]. This results in a step in the calculated vertical spectra midway through the descending range. The length of the step increases with decreasing V/H. The step terminates at $T_V = 0.5$ s for all V/H but begins at $T_V = 0.49$ for $V/H = 1.2$, $T_V = 0.4$ for $V/H = 1.0$ and $T_V = 0.275$ for $V/H = 0.75$ (Fig. 3). This step in the response spectrum does not represent the real motion, which consequently leads to difficulty in fitting the motions to the target spectra.

3. Ground Motion Selection and Scaling

To study the effect of intense vertical shaking on the structural response, ground motions with relatively large vertical components were hand selected to represent the target spectra. Initially, 92 recorded motions were selected from the PEER NGA database

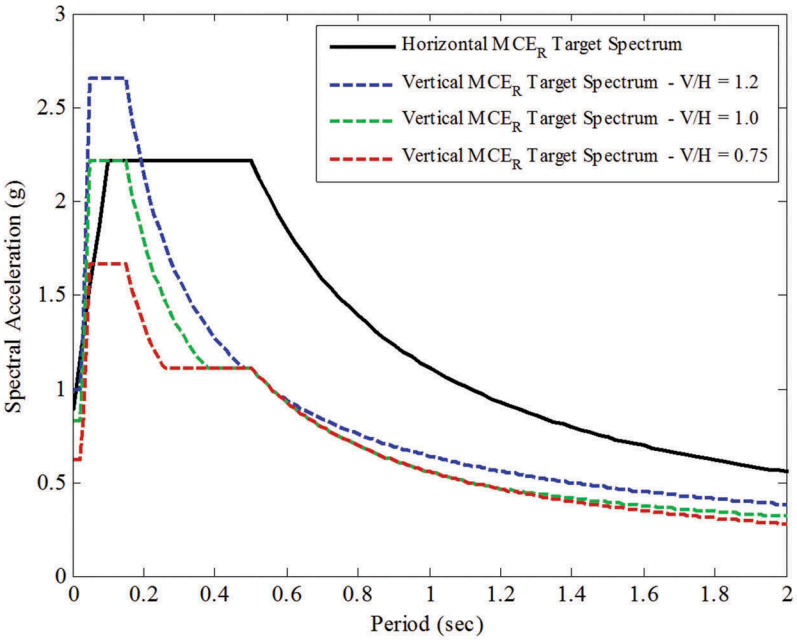

Figure 3. Horizontal and vertical MCE_R spectra with 5% damping.

[Chiou *et al.*, 2008] by identifying ground motion triplets that by inspection best matched the shape and relative intensity of the target spectra for different V/H. These motions were amplitude scaled to minimize the sum of the squared error between the response spectrum of the ground motion component and the target spectrum in each direction. The error was minimized over a period range from 1.5 to 4.0 s in both horizontal directions and from 0 to 2.0 s in the vertical direction. The broad period range encompassed the parameter variation considered in the study. All three components were scaled by a single-scale factor to preserve the relative component amplitudes of the original recorded motion as recommended by commentary of ASCE 7–16 [ASCE, 2016].

These 92 motions were filtered to select three subsets of 12 motions, one for each V/H ratio, to be used in the analysis. The number of motions per subset was limited because identifying motions that matched the target spectrum well in all directions using a single-scale factor was found to be difficult. First, motions requiring scale factor >3.0 were removed to exclude ground motion distortion effects that may come from excessive scale factors. Then multiple attempts were made by trial and error to choose a smaller set of 12 motions with median spectra that matched the target spectra in both horizontal and vertical directions. This process was repeated for each V/H ratio. The final ground motion suite selected for the site contains 36 scaled ground motions, divided into three subsets of 12 for different V/H ratios. The suite contains 18 unique records, as some records are repeated. Table 1 summarizes the selected ground motions and the calculated scale factors to match horizontal and vertical target spectra for V/H = 1.2, 1.0 and 0.75. Six motions are common in all three subsets, while five motions are used in both the first and second subsets, and only one motion is mutual in the first and third subsets.

Table 1. Selected ground motions and scale factors for horizontal and vertical target spectra with different *V/H* ratios.

No.	Earthquake name	Year	Station name	Scale factor		
				V/H = 1.2	*V/H* = 1.0	*V/H* = 0.75
1	San Fernando	1971	Pacoima Dam (upper left abut)	–	1.44	–
2	Tabas, Iran	1978	Tabas	1.22	1.2	1.17
3	San Salvador	1986	Geotech Investig Center	2.67	2.59	–
4	Loma Prieta	1989	LGPC	1.13	1.11	–
5	Manjil, Iran	1990	Abbar	1.81	1.7	1.62
6	Cape Mendocino	1992	Cape Mendocino	–	–	1.54
7	Northridge	1994	LA – Sepulveda VA Hospital	2.16	2.12	2.07
8	Northridge	1994	Beverly Hills – 14145 Mulhol	2.29	2.22	–
9	Northridge	1994	Jensen Filter Plant Generator Building	1.32	1.3	–
10	Kobe, Japan	1995	Amagasaki	–	–	2.07
11	Chi-Chi, Taiwan	1999	TCU071	2.52	2.41	2.31
12	Chi-Chi, Taiwan	1999	TCU072	2.41	–	2.25
13	Chi-Chi, Taiwan	1999	TCU079	2.98	2.81	–
14	Chuetsu-oki	2007	Kashiwazaki Nishiyamacho Ikeura	–	–	2.03
15	Chuetsu-oki	2007	Kashiwazaki NPP Unit 5: ground surface	1.65	1.63	1.6
16	L'Aquila, Italy	2009	L'Aquila – Parking	2.88	2.72	2.63
17	El Mayor-Cucapah	2010	Cerro Prieto Geothermal	–	–	1.6
18	El Mayor-Cucapah	2010	Calexico – Fire Station	–	–	2.69

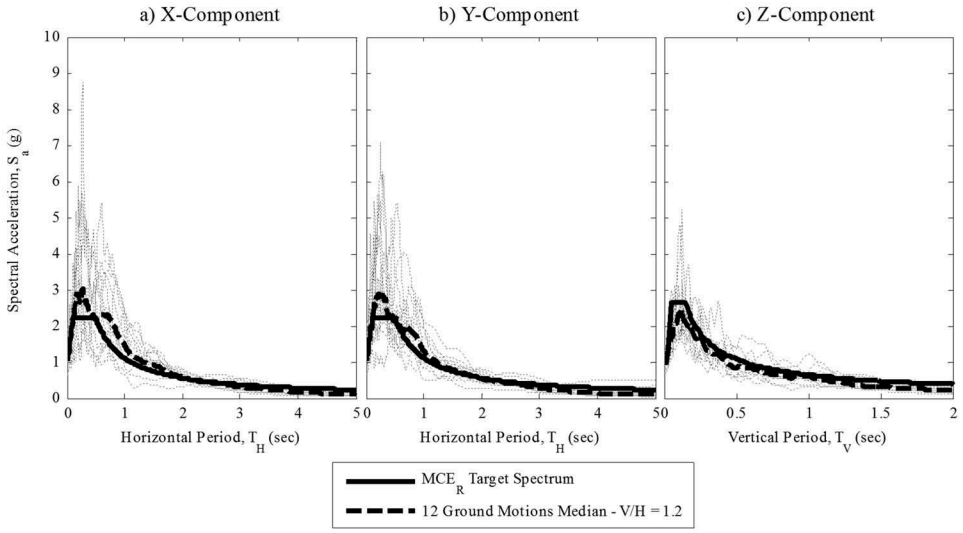

Figure 4. The 5% damped acceleration response spectra for 12 scaled ground motions, median spectrum and MCE_R target spectrum for *V/H* = 1.2: (a) *X* component, (b) *Y* component and (c) *Z* component.

Figure 4 shows the *X*, *Y* and *Z* components of the 12 scaled motions and median spectra, plotted against the target MCE_R horizontal and vertical spectra with $V/H = 1.2$. The *X* component of the median spectrum is greater than *Y* component for $T_H < 2$ s, but the two are almost the same for $T_H > 2$ s. For this reason, only *X* and *Z* components are presented in the analysis hereafter. Figure 5 compares the target spectrum and the median spectrum of the 12 ground motions for different *V/H* ratios. As discussed previously, the step in the vertical target spectrum made matching the ground motions challenging. As a

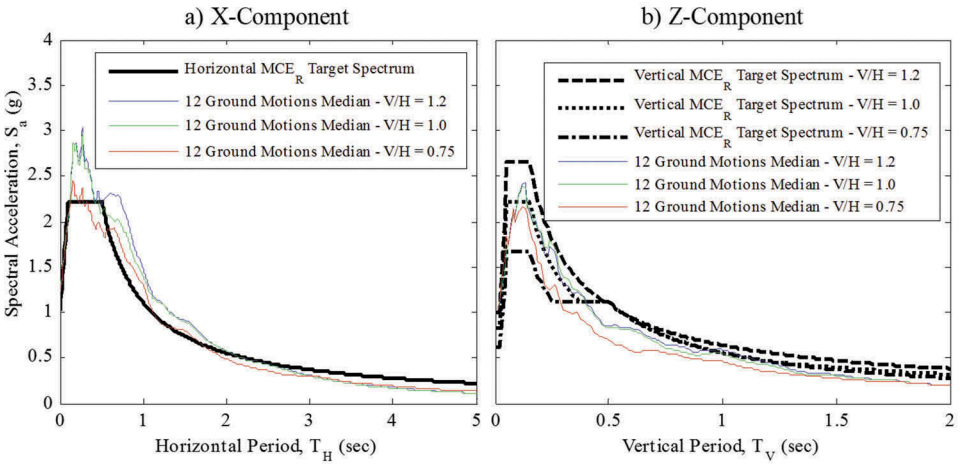

Figure 5. Median 5% damped acceleration spectra of the scaled motions compared to MCE_R target spectra for various *V*/*H* ratios: (a) *X* component and (b) *Z* component.

result, the discrepancy between the median and target spectra is relatively large and increases with decreasing *V*/*H*.

4. Rigid Block Model

4.1. *Model Assumptions and Equations*

A simplified 2D rigid block model was developed to understand the fundamental dynamics of combined horizontal and vertical isolation. This block is supported on isolation bearings at each base corner, represented by linear springs with total horizontal stiffness (K_H) and vertical stiffness (K_V), as shown in Fig. 6. The block has mass (m) and moment of inertia (I_θ) lumped at the geometric center, which is the center of mass (CM). The model degrees of freedom (DOFs) are horizontal displacement (U_X), vertical displacement (U_Z) and rotation (θ) of the block at its CM (Fig. 6). The coupled equations of motion for the system subjected to horizontal and vertical ground accelerations $\ddot{U}_{gx}(t)$ and $\ddot{U}_{gz}(t)$ are as follows:

$$\begin{bmatrix} m & 0 & 0 \\ 0 & m & 0 \\ 0 & 0 & I_\theta \end{bmatrix} \begin{Bmatrix} \ddot{U}_X(t) \\ \ddot{U}_Z(t) \\ \ddot{\theta}(t) \end{Bmatrix} + [C] \begin{Bmatrix} \dot{U}_X(t) \\ \dot{U}_Z(t) \\ \dot{\theta}(t) \end{Bmatrix} + \begin{bmatrix} K_H & 0 & K_H * h/2 \\ 0 & K_V & 0 \\ K_H * h/2 & 0 & K_H * h^2/4 + K_V * b^2/4 \end{bmatrix} \begin{Bmatrix} U_X(t) \\ U_Z(t) \\ \theta(t) \end{Bmatrix} = -\begin{bmatrix} m & 0 & 0 \\ 0 & m & 0 \\ 0 & 0 & I_\theta \end{bmatrix} \begin{Bmatrix} \ddot{U}_{gx}(t) \\ \ddot{U}_{gz}(t) \\ 0 \end{Bmatrix} \quad (1)$$

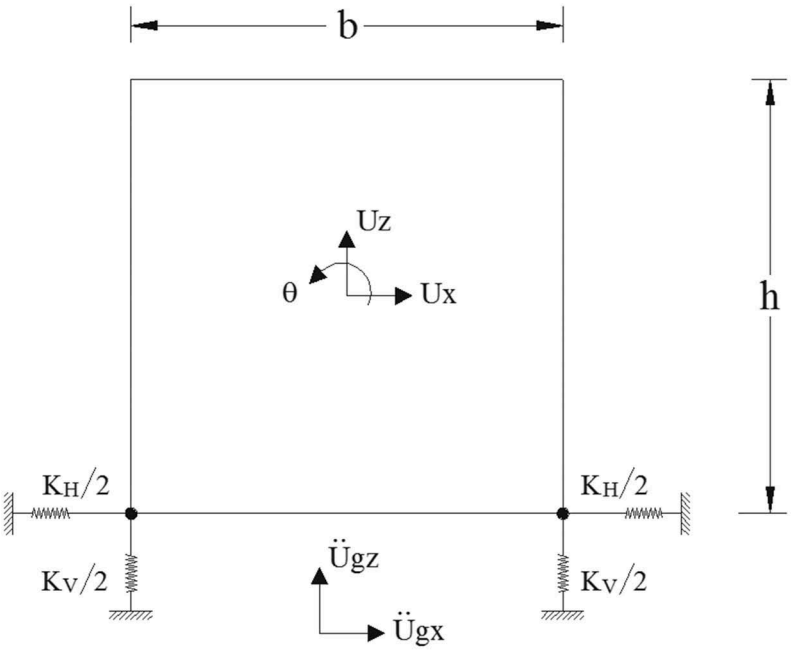

Figure 6. Rigid block used in MATLAB analysis.

The damping matrix C is defined based on Rayleigh damping calibrated for target damping ratios in the horizontal (first) and vertical (second or third) modes. According to the stiffness matrix, horizontal translation and rocking are coupled, while the vertical translation is uncoupled from the other two modes. The equations of motion are solved numerically in MATLAB using Newmark's linear acceleration method (γ = 1/2 and β = 1/6) with a time increment equal to the time step of the recorded ground motion.

4.2. *Validation of Rigid Block Modeling Approach*

A multistory frame model was developed and analyzed using SAP2000 to validate the applicability of the simplified rigid block model to represent a flexible frame building with an isolation system. The model was a five-story single-bay plane frame with story height 3.6 m and bay width 9 m, consistent with an overall height-to-width or aspect ratio (h/b) = 2 of the rigid block. The frame was modeled using linear steel frame elements with lumped mass in the middle of each floor beam. Wide flange sections W1100 x 499 and W610 x 372 were used beams and columns, respectively. The two joints on each floor were connected with rigid constraint to eliminate local deformation; thus, the frame behaved as a shear frame with rigid beams. Lumped mass values were m = 175 kN s^2/mm at each floor, except the roof, where m/2 was applied. Linear link elements were applied at the frame base to model the isolation system. The stiffness of the links was defined to represent isolation period in both horizontal and vertical directions, while the rotation DOF was fixed, and the damping was set to be zero. Both rigid (R) and flexible (F) frame models were investigated to evaluate the influence of frame flexibility on accuracy of the

rigid block model. The fixed-base properties were $T_{H,R}$ = 0.5 s, $T_{V,R}$ = 0.1 s for the rigid frame, while for the flexible frame were $T_{H,F}$ = 1.0 s, $T_{V,F}$ = 0.2 s.

The isolation system used in both models had T_H = 3.0 s, and different values were considered for T_V: 0.1, 0.5, 1.0 and 2.0 s. Constant damping of 5% was assigned for all higher modes. However, damping overrides were applied to the first three modes according to the following: 20% for both fundamental horizontal and vertical modes and damping for the intermediate rocking mode calculated using the Rayleigh quotient. The damping in the multistory frame model was selected to best match the applied viscous damping for the rigid block model, assumed to correspond to 20% damping ratio in both the horizontal and vertical modes based on a rigid superstructure assumption.

Table 2 compares the first three modal periods of the multistory rigid frame and rigid block models for the different vertical isolation periods considered. The respective periods of the two different models differ by no more than 10%; except when T_V = 0.1 s, the second and third mode periods differ by nearly 50% and 30%, respectively. The rigid block approach does not account for the superstructure flexibility that is present in the multistory frame model; thus, the periods obtained from multistory frame model exceed the ones calculated from rigid block approach. As expected, the influence of the superstructure flexibility is more significant when the isolation period is smaller. Therefore, the modal periods of the multistory frame and rigid block differ most when T_V = 0.1 s; however, the discrepancy decreases when the vertical period increases.

The first mode in the rigid block and multistory frame models is mainly horizontal translation accompanied by a relatively small rocking angle as presented in Fig. 7a and 8a, respectively. The second mode in the rigid block model is governed by rocking

Table 2. First three modal periods of the multistory rigid frame and rigid block models.

	Multistory rigid frame model			Rigid block model		
	Mode period (s)			Mode period (s)		
Case	Mode 1	Mode 2	Mode 3	Mode 1	Mode 2	Mode 3
T_H = 3.0 s, T_V = 0.1 s	3.1150	0.2721	0.1439	3.0067	0.1288	0.1
T_H = 3.0 s, T_V = 0.5 s	3.3135	0.6778	0.5208	3.1691	0.6111	0.5
T_H = 3.0 s, T_V = 1.0 s	3.9328	1.0876	1.0233	3.6825	1.0517	1.0
T_H = 3.0 s, T_V = 2.0 s	5.9353	2.0375	1.4188	5.4445	2.0	1.4227

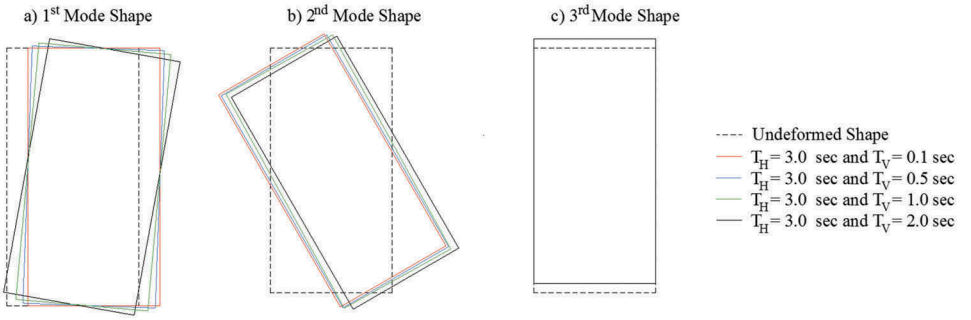

Figure 7. Mode shapes for rigid block model with different vertical isolation period T_V: (a) first mode shape, (b) second mode shape and (c) third mode shape.

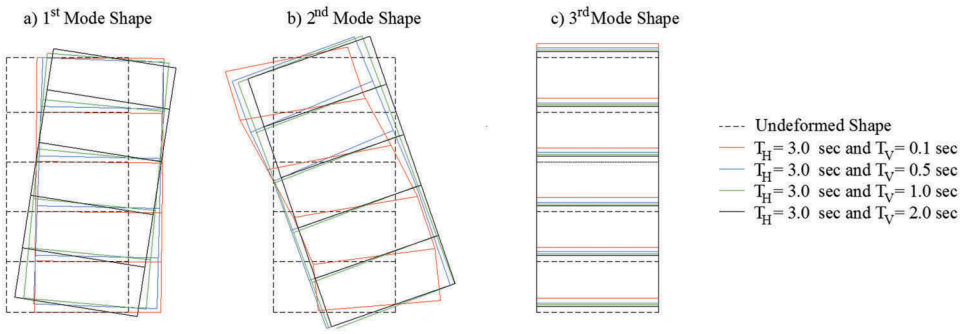

Figure 8. Mode shapes for multistory rigid frame model with different vertical isolation period T_V: (a) first mode shape, (b) second mode shape and (c) third mode shape.

with small horizontal translation (Fig. 7b), while the multistory frame model sees height-based fluctuations in story drift ratio, but the overall modes are comparable with the rigid block model (Fig. 8b). In both models, the third mode is pure vertical translation without any rocking (Fig. 7c and 8c). The resulting mode shapes obtained from both the multistory frame and the rigid block models have the characteristic that horizontal and rocking displacements are coupled, but vertical displacement is uncoupled from rocking. Therefore, the simplified rigid block model represents the dynamics of a multistory frame model. Also, the coupling increases as T_V increases, which is observed as increasing rocking in the horizontal mode and increasing horizontal translation in the rocking mode. In both rigid block and frame models, the second mode is the rocking mode and the third mode is the vertical mode up until T_V = 1.0 s. However, the vertical and rocking modes switch to the second and third modes, respectively, when T_V = 2.0 s (Table 2).

Three representative ground motions (#2, 7 and 12) scaled to the target spectra for V/H = 1.2 were applied to both the rigid block and multistory frame models to compare their responses. History of roof drift ratio (in percentage), vertical displacement and total acceleration at the bearing are compared for the rigid block and multistory rigid frame model in Fig. 9–11, respectively, for each value of T_V for ground motion (#7). For the rigid block model, drift ratio was computed as the ratio of relative horizontal displacement to the block height, which is shown to simplify to the rotation θ:

$$\text{Driftratio} = \frac{(U_{XTop} - U_{XBottom})}{h} = \frac{[U_X - (h/2)\theta] - [U_X + (h/2)\theta]}{h} = -\theta \qquad (2)$$

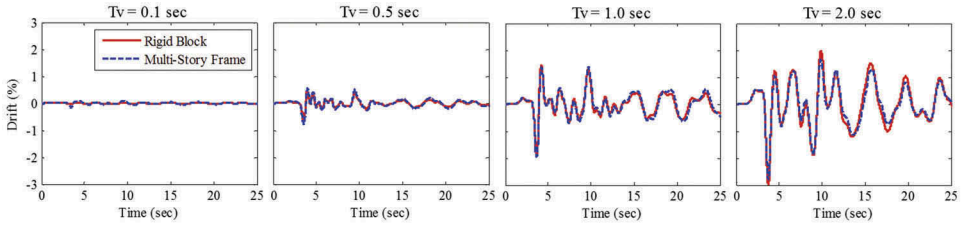

Figure 9. Roof drift ratio of rigid block and multistory rigid frame for various T_V.

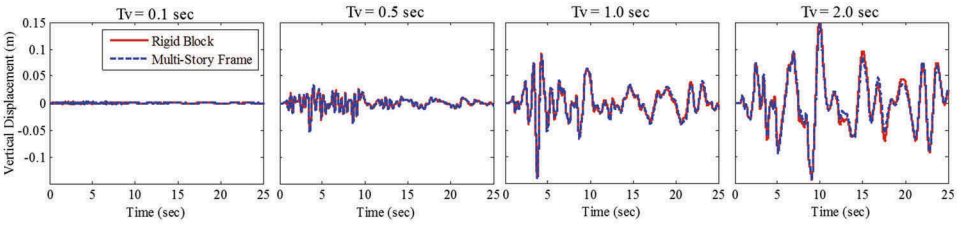

Figure 10. Bearing vertical displacement for rigid block and multistory rigid frame for various T_V.

In Eq. (2), U_{XTop} is the horizontal displacement at the top of the rigid block and $U_{XBottom}$ is the horizontal displacement at the bearing. For the multistory frame model, the drift ratio was computed as total relative superstructure displacement from base to roof over total height. Visually, the two models are closely correlated, as the discrepancy between the response histories is minor. Also, for both models, the rocking effect, as represented by drift ratio (noted earlier in the mode shapes), and the vertical displacement increase as T_V increases in Fig. 9 and 10, respectively. Discrepancy between the two models' responses at T_V = 0.1 s is noted, especially for vertical acceleration. Discrepancies in response of the two models shown in Fig. 9–11 coincide with the discrepancy in the calculated periods, as discussed previously.

The following error measures were calculated for the three applied ground motions to better quantify the error in the rigid block model relative to the multistory frame models. The normalized root mean square deviation (NRMSD) is the RMSD normalized by maximum peak-to-peak response:

$$\mathrm{RMSD} = \sqrt{\frac{1}{\mathrm{N}}\sum_{\mathrm{i}=1}^{\mathrm{N}}\left(r_{i,B} - r_{i,M}\right)^2} \tag{3}$$

$$\mathrm{NRMSD} = \frac{\mathrm{RMSD}}{r_{max,\,M} - r_{min,\,M}} \tag{4}$$

where r = response quantity of interest (drift, vertical displacement and acceleration), i = ith step, N = number of steps, B refers to rigid block and M refers to multistory frame. NRMSD is a measure of average relative error in the response over the history. The peak error, or relative error in the peak responses, was computed as follows:

$$Peak\ Error = \frac{max_i\left|r_{i,B}\right| - max_i\left|r_{i,M}\right|}{max_i\left|r_{i,M}\right|} \tag{5}$$

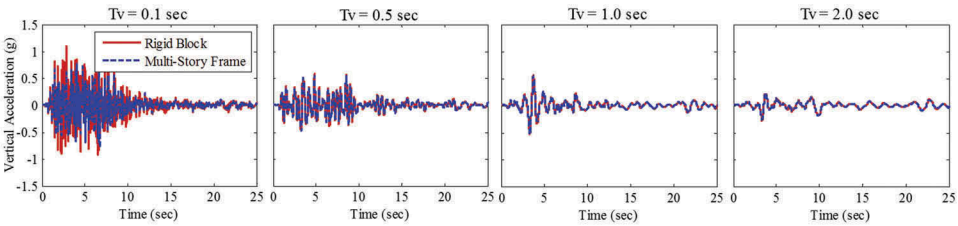

Figure 11. Bearing vertical acceleration for rigid block and multistory rigid frame for various T_V.

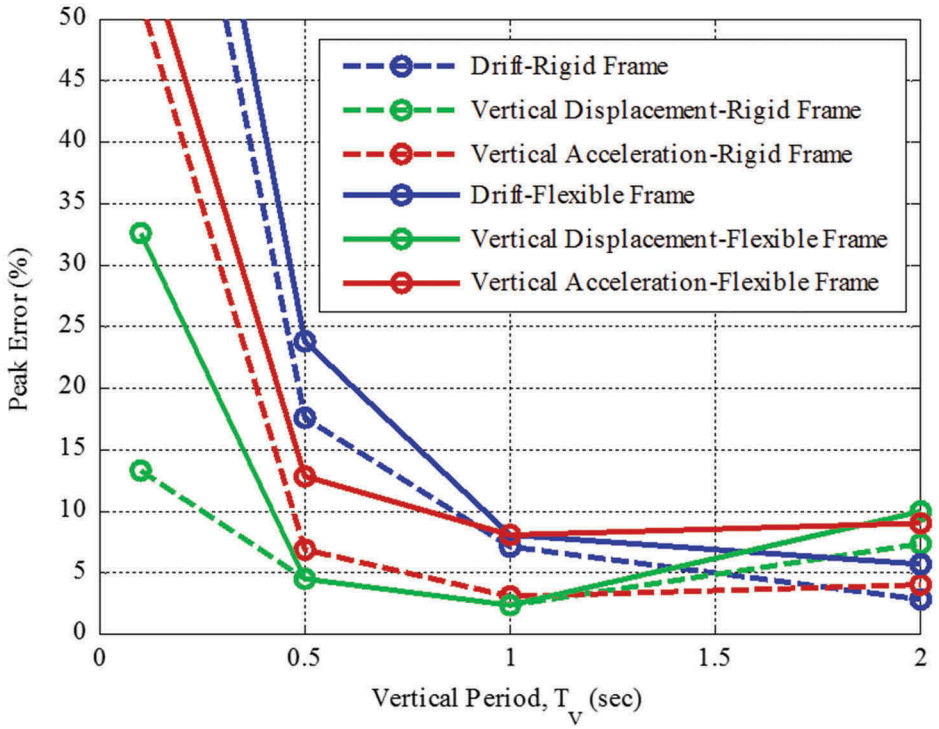

Figure 12. Peak error in rigid block response relative to multistory frame response as a function of T_V.

The average peak error and NRMSD obtained from the three applied ground motions for the drift ratio, vertical displacement and acceleration as a function of the vertical isolation period for the two frame models are presented in Fig. 12 and 13, respectively. According to peak error and NRMSD calculations, the error in the rigid block model is maximized when T_V = 0.1 s, for reasons discussed previously. The rigid block is a good simplified representative model of the response of a multistory frame with horizontal and vertical isolations as the error quantity never rises above 25% for the peak error and 6% for NRMSD for $T_V \geq 0.5$ s. However, the increase in the frame flexibility slightly increases the error between the rigid block and frame model. Furthermore, the correspondence between computed rotation θ of the rigid block and base to roof drift in the multistory frame model confirms that the rotation of the rigid block is a good measure of overall drift, to be used with caution as the superstructure becomes more flexible.

5. Parametric Study of Rigid Block Model

A parametric study was carried out to investigate the effect of different parameters on the isolation performance. Considered parameters include T_H, T_V, V/H, site class, damping ratio (ζ) and h/b.

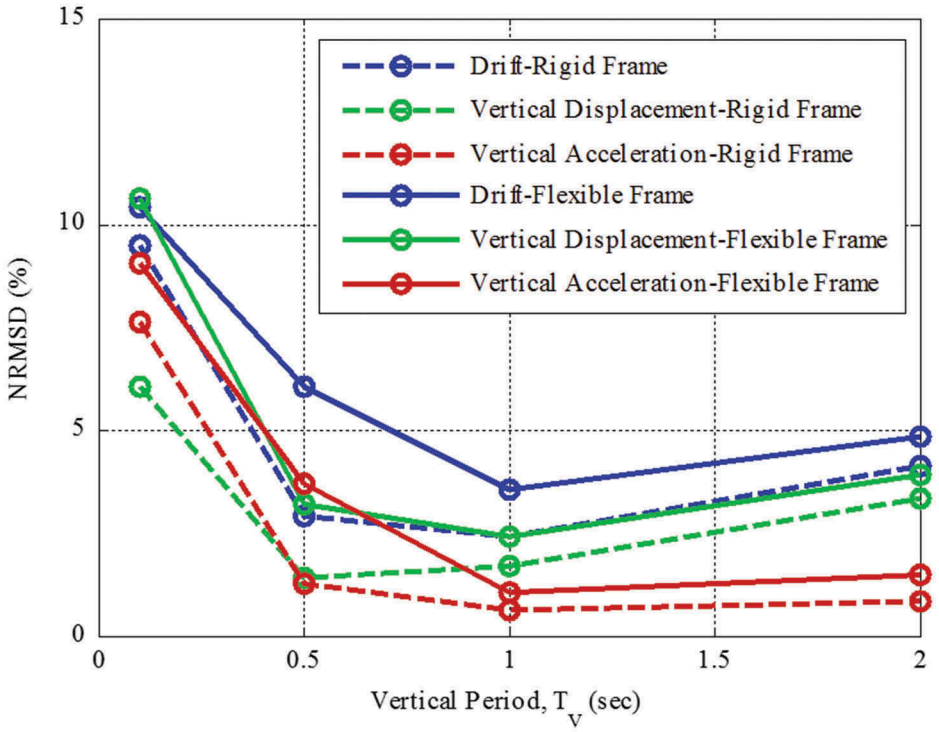

Figure 13. Normalized error in rigid block response relative to multistory frame response as a function of T_V.

5.1. Effect of Varying Both T_H and T_V

The response trends of the rigid block are investigated for different combinations of horizontal and vertical isolation periods. Peak responses are presented for the ground motion subset for $V/H = 1.2$ as a function of horizontal period T_H varying from 0 to 5 s. Peak responses are presented for each individual excitation; also shown are the median μ, $\mu + 1\sigma$ (84^{th} percentile), and $\mu - 1\sigma$ (16^{th} percentile) over the ground motion subset, where σ is the standard deviation, to summarize the variation with ground motions. In general, $T_H < 1$ s represents the response of a comparable fixed base structure. As before, discrete values of $T_V = 0.1$, 0.5, 1.0 and 2.0 s are considered, $\zeta = 20\%$ is applied in the horizontal and vertical modes and aspect ratio $h/b = 2$. The resulting peak horizontal base displacement (isolator displacement), peak drift ratio (in percentage) and peak vertical displacement at the left bearing are shown in Fig. 14–16, respectively.

As expected, the bearing horizontal displacement increases with increasing T_H (Fig. 14). However, for a given T_H, bearing displacement decreases for higher values of T_V. Note that the bearing horizontal displacement is influenced by both U_X and θ. The rocking effect – represented by θ – increases with increasing T_V, which causes the bearing horizontal displacement to decrease while the roof horizontal displacement increases. The drift ratio (Fig. 15) decreases with increasing T_H but is also correlated to

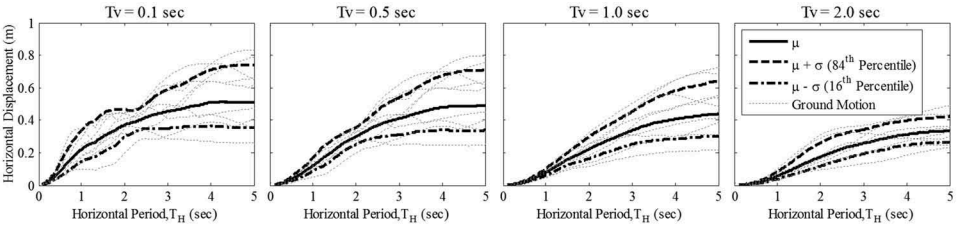

Figure 14. Horizontal base displacement (isolator displacement) for V/H = 1.2 and different T_V.

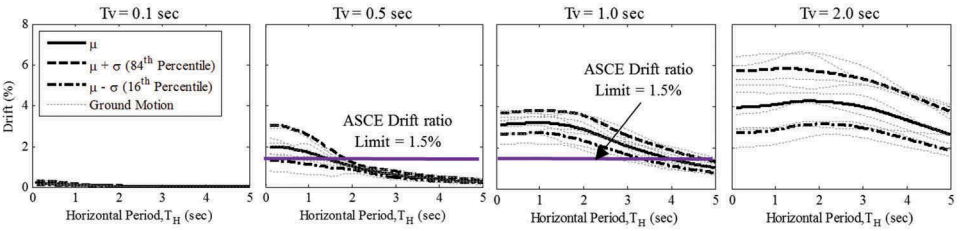

Figure 15. Relative drift ratio between top and bottom of the block for V/H = 1.2 and different T_V.

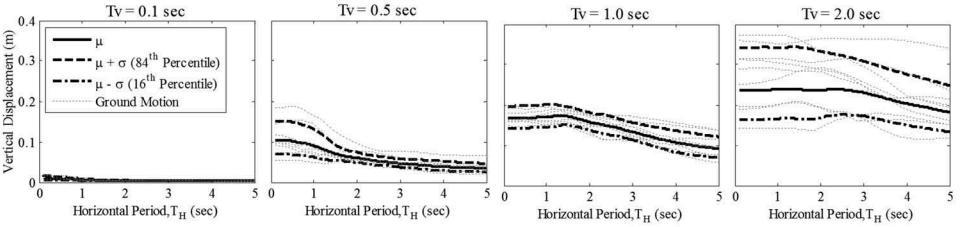

Figure 16. Vertical displacement at left bearing for V/H = 1.2 and different T_V.

T_V. Also, the vertical bearing displacement is closely correlated to the drift ratio as shown in Fig. 16. Both the bearing vertical displacement and the drift ratio follow the trend for rocking θ and thus increase as T_V increases. Furthermore, vertical displacement at the block center is unaffected by T_H; thus, variation in bearing vertical displacement with T_H is due to rocking alone. Large drift ratios result even at short periods T_H when vertical flexibility is introduced (T_V = 0.5, 1 or 2 s). In each case, the drift ratio and vertical displacement are almost constant up to $T_H = T_V$. However, they eventually decrease as T_H increases beyond T_V. This suggests that for effective design, T_H and T_V should not be closely coupled, and T_H should be selected to be much longer than T_V. An isolated building designed per ASCE 7–16 is designed to remain linear under the design lateral forces and not exceed a drift limit of 1.5% [ASCE, 2016]. Therefore, the drift ratio demand of the rigid block is evaluated against this code limit of 1.5%. Thus, T_V = 0.5 s produces acceptable results for almost all T_H, T_V = 1.0 s produces acceptable drift ratios for $T_H > 3.5$ s and T_V = 2 s produces drift ratios higher than the ASCE limit for all values of T_H.

The 16th and 84th percentile curves represent bounds for the middle 68% of the expected response. Responses with low dispersion (small difference between 16th and 84th percentile) are predicted with more confidence than those with high dispersion (large difference between 16th and 84th percentile). The results show that both drift ratio and bearing vertical displacement are predicted with increasing confidence as T_H increases and as T_V increases. However, the opposite is true for the bearing horizontal displacement. The choice of suitable T_V will also be influenced by the ability of the isolation system to accommodate the displacement and reliably limit the maximum drift ratio below the acceptable design threshold; therefore, design within the low dispersion range is preferred.

Horizontal acceleration amplification factors, $A_{Amp,H}$ (peak horizontal acceleration in the structure normalized by horizontal peak ground acceleration (PGA)) are illustrated in Fig. 17 for the top (representative of the roof) and base of the block. $A_{Amp,H} < 1$ indicates that horizontal acceleration is attenuated or reduced compared to PGA. $A_{Amp,H}$ at the top exceeds that at the base when $T_H \leq 1.0$ s and $T_V = 0.1$ s, representative of fixed base. However, when $T_H > 1.0$ s and $T_V = 0.1$ s – representative of a conventional isolated building – $A_{Amp,H}$ is nearly constant over the structure height due to the absence of rocking and decreases with increasing T_H. For a 3D isolation system ($T_H > 1.0$ s and $T_V > 0.5$ s), $A_{Amp,H}$ at the top of the block is lower than $A_{Amp,H}$ at the base. The rocking of the structure causes this effect as the rocking mode acts in the opposite direction of the horizontal mode and thus counteracts the movement at the top as illustrated previously in Fig. 7. The horizontal acceleration attenuates as T_H increases, and a change in T_V has insignificant influence on the horizontal acceleration after T_H is sufficiently long (Fig. 17). For example, at $T_H = 3.0$ s, $A_{Amp,H} \approx 0.25$ regardless of vertical period.

The vertical acceleration amplification factor, $A_{Amp,V}$ (peak vertical acceleration at the block edge normalized by vertical peak ground acceleration or PGA_Z) is presented in Fig. 18. In the range of typical horizontal isolation periods ($T_H \geq 2.0$ s), $A_{Amp,V}$ is not affected by T_H variation and is inversely proportional to T_V as observed in Fig. 18. $A_{Amp,V} < 1$ means vertical acceleration is attenuated or reduced compared to PGA_Z. For $T_V = 0.5$ s, attenuation of vertical acceleration may be achieved, but it is not reliable. However, for both $T_V = 1.0$ and 2.0 s, reliable attenuation of vertical acceleration can be achieved. Therefore, vertical acceleration attenuation can be achieved by increasing T_V and hence the bearing flexibility, but the limiting factors are the vertical displacement and drift ratio.

In summary, 3D isolation helps limit horizontal and vertical accelerations and corresponding forces in the structure resulting from the applied ground motion. Based on the results presented herein, the acceptable range of 3D isolation periods is concluded to be $T_V = 0.5$ s

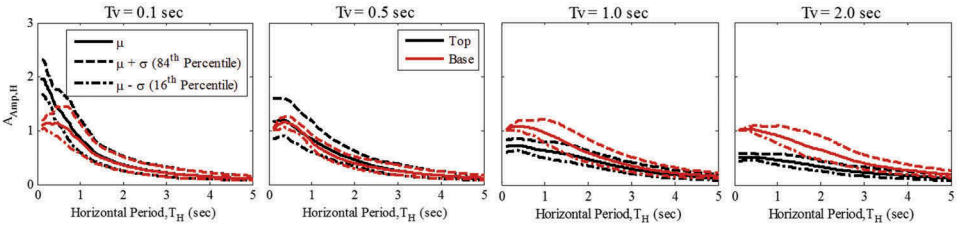

Figure 17. $A_{Amp,H}$ at the top and base of the block for $V/H = 1.2$ and different T_V.

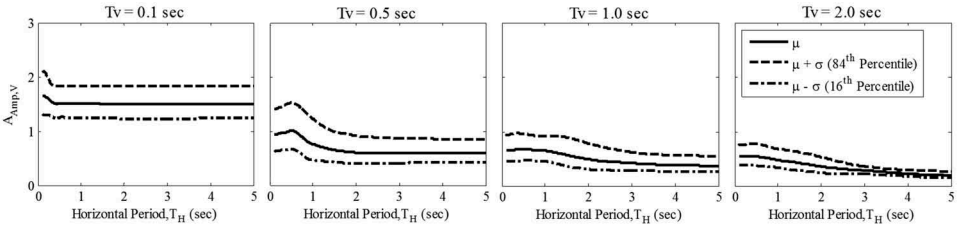

Figure 18. $A_{Amp,V}$ at the block edge for V/H = 1.2 and different T_V.

and $T_H \geq 1.5$ s or $T_V = 1.0$ s and $T_H \geq 4.0$ s, and intermediate periods as determined by interpolation. These ranges have been selected (a) to keep drift ratio below ASCE limit [ASCE, 2016] (b) to attenuate both horizontal and vertical accelerations and (c) to achieve good separation of horizontal and vertical isolation periods so as to minimize rocking.

5.2. *Effect of Varying Site Conditions*

Peak responses for various V/H ratios and site classes are compared to investigate the variability of 3D isolation system response in different site conditions. As discussed previously in Section 2, V/H ratio = $0.8C_V$ where C_V is a vertical coefficient that depends on S_S and site class. Also, the target spectra vary as a function of site class. Next, two sets of analyses are presented to study the effect of different site conditions. First, rigid block responses are compared for V/H = 1.2, 1.0 and 0.75 for the same site parameters S_S, S_1 and site class D. For these analyses, different ground motions were selected and scaled to match the target spectra as described previously in Section 3. The rigid block was modeled with damping ratios ζ = 20% in the horizontal and vertical modes and aspect ratio h/b = 2.

Median (over the ground motion subsets) of the peak values of drift ratio, vertical displacement at the left bearing, $A_{Amp,H}$ and $A_{Amp,V}$ for different V/H ratios are presented in Fig. 19–22. The responses are presented only for T_V = 0.5 and 1.0 s based on the conclusions in the previous

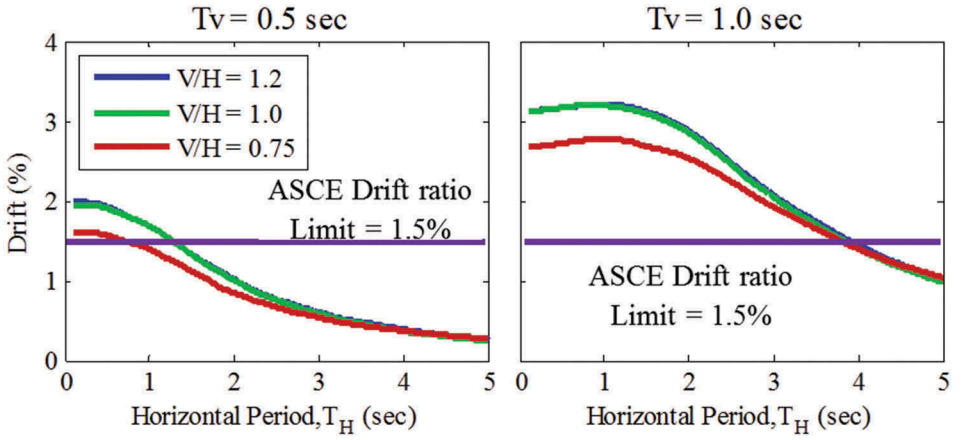

Figure 19. Relative drift ratio between top and bottom of the block for different V/H ratios.

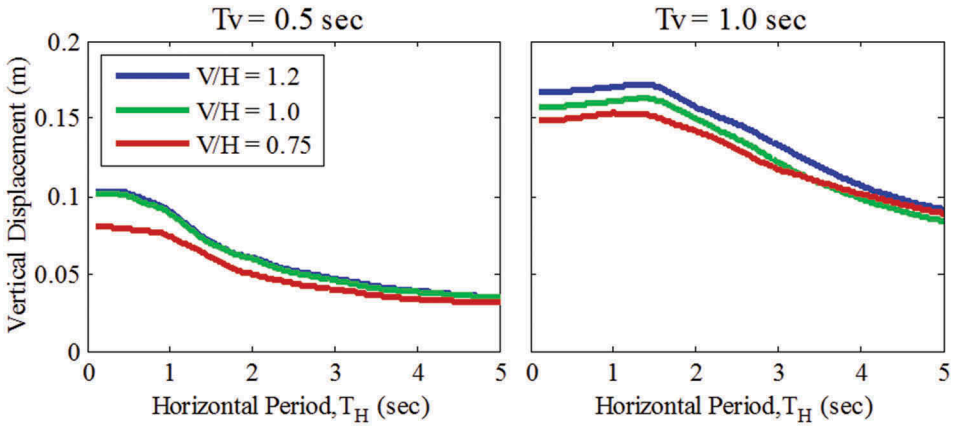

Figure 20. Vertical displacement at left bearing for different *V*/*H* ratios.

section. Drift ratio and bearing vertical displacement responses are seen to depend only weakly on *V*/*H* ratios (Fig. 19 and 20), while the acceleration amplification factors are independent of *V*/*H* ratios (Fig. 21 and 22). The obtained results may be a reflection of the ground motion selection and scaling procedures and not a true evaluation of theoretical differences between different *V*/*H* ratios. Although best practice methods were used, several of the selected motions were common among multiple suites, and the scale factors differed only slightly between suites, as presented in Table 1. However, to fit any of the target spectra, the chosen ground motions all had large vertical intensities compared to typical motions in the database.

Some distinction between $V/H = 0.75$ and the two larger V/H ratios is apparent (Fig. 19 and 20). In particular, drift ratio and bearing vertical displacement for $V/H = 0.75$ are lower than for $V/H = 1.2$ and 1.0 when $T_H < 3.0$ s. The acceptable range of 3D isolation periods found in Section 5.1 for $V/H = 1.2$, based on the limitations specified previously, can be applied to all V/H ratios.

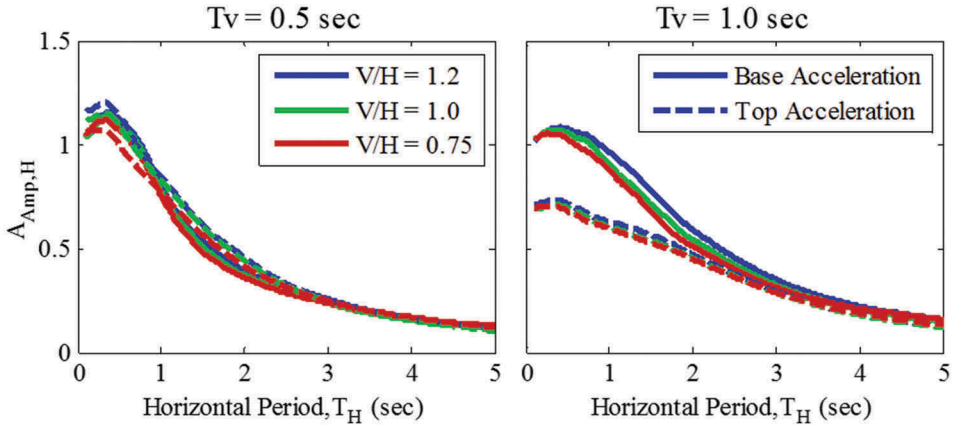

Figure 21. $A_{Amp,H}$ at the top and base of the block for different *V*/*H* ratios.

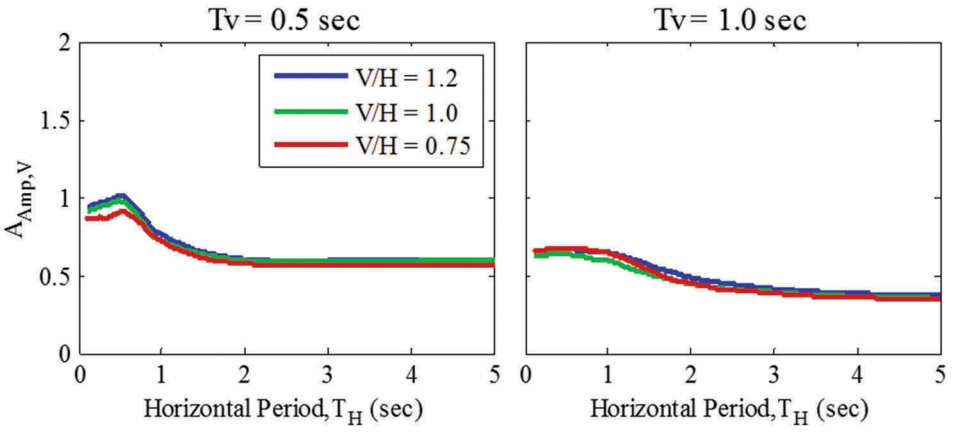

Figure 22. $A_{Amp,V}$ at the block edge for different V/H ratios.

The second set of analyses – presented next – varies the site class while holding S_S, S_1 and V/H constant. The original hypothetical site was classified as site class D (stiff soil). Site classes C (very dense soil/soft rock) and E (soft clay soil) are considered to investigate the isolation behavior with different soil types. In these analyses, ground motions selected previously for V/H = 1.2 were scaled to match the new target spectra presented in Fig. 23.

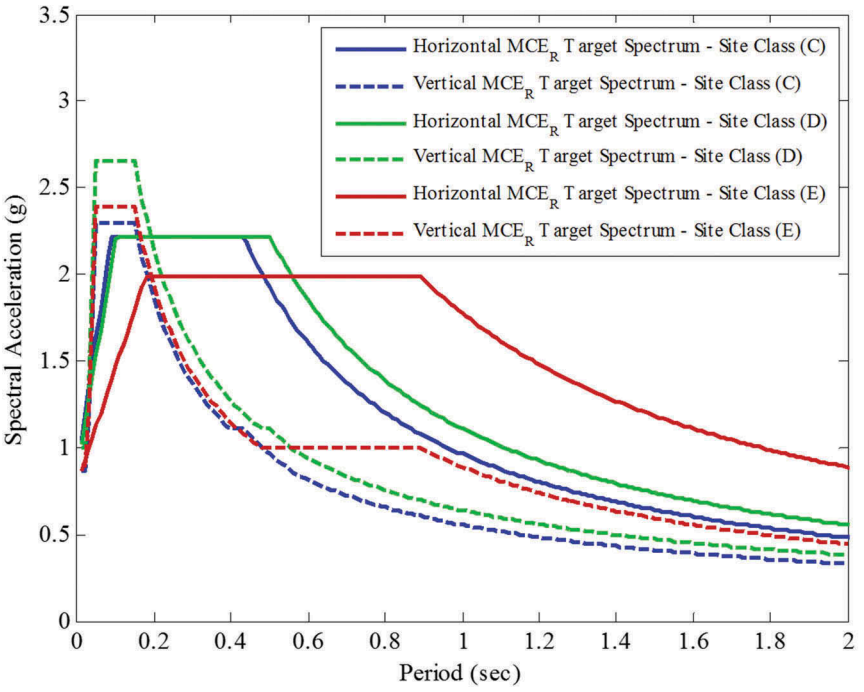

Figure 23. Horizontal and vertical MCE_R spectra with 5% damping for different site classes.

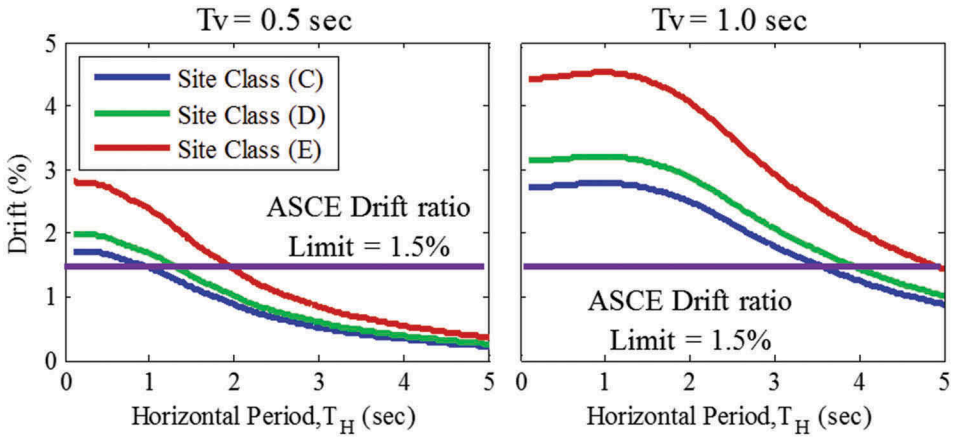

Figure 24. Relative drift ratio between top and bottom of the block for different site classes.

Again, the rigid block model was modeled with damping ratios $\zeta = 20\%$ in the horizontal and vertical modes and aspect ratio $h/b = 2$.

Median (over the ground motion subsets) of the peak values of drift ratio, vertical displacement at the left bearing, $A_{\mathrm{Amp,H}}$ and $A_{\mathrm{Amp,V}}$ for different site classes are presented in Fig. 24–27. All responses are seen to increase for increasing site class (increasingly softer soil) over the entire parameter range. The increase in response in site class E compared to D is most pronounced, likely due to significant lengthening of the constant acceleration region of the horizontal spectrum (and corresponding lengthening of the "step" region of the vertical spectrum). The results suggest that a more limited range of horizontal and vertical isolation periods would satisfy acceptable drift limits for site class E due to the change in spectral shape.

The results suggest that the key isolator and structural response parameter trends are not much affected by site parameters S_S and S_1; rather, governing system parameters and

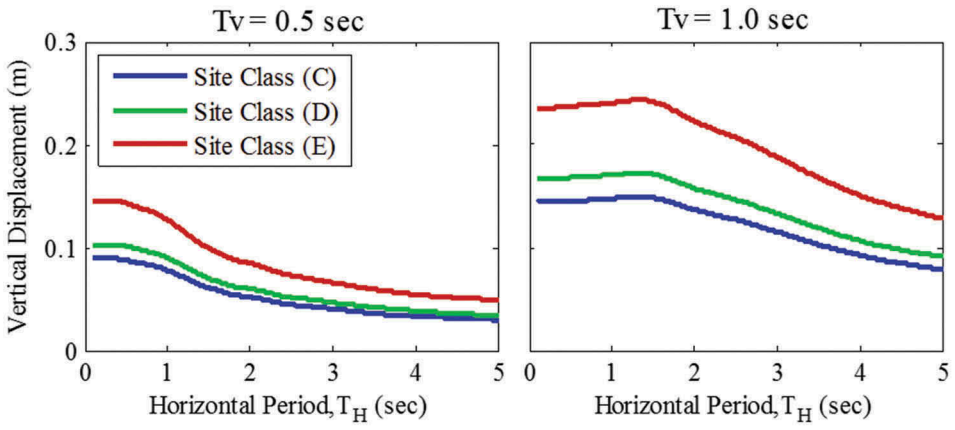

Figure 25. Vertical displacement at left bearing for different site classes.

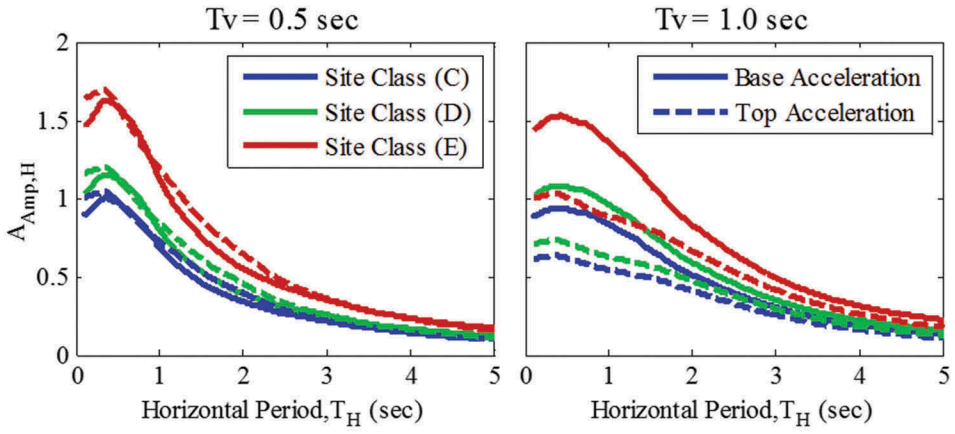

Figure 26. $A_{Amp,H}$ at the top and base of the block for different site classes.

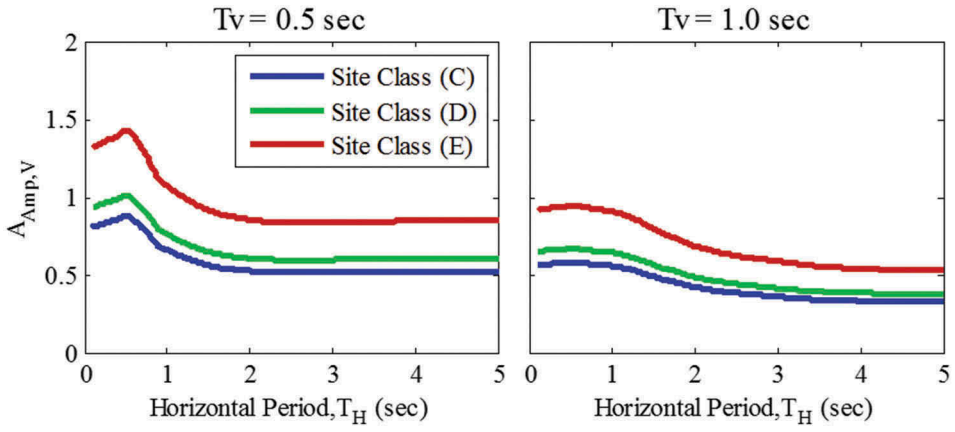

Figure 27. $A_{Amp,V}$ at the block edge for different site classes.

site class – which highly influences spectral shape – are much more influential. The subsequent analyses will consider only ground motions selected and scaled to match target spectra with $V/H = 1.2$ and for site class D.

5.3. *Effect of Viscous Damping*

The influence of variable viscous damping on the response of the rigid block is investigated next. For this analysis, isolation periods were selected as $T_H = 3.0$ and 5.0 s and $T_V = 0.5$ and 1.0 s (all four combinations were considered), and the aspect ratio of the rigid block model was $h/b = 2$. Median (over the ground motion subsets) of the peak values of drift ratio, left bearing vertical displacement, $A_{Amp,H}$ and $A_{Amp,V}$ are presented in Fig. 28–31. The damping ratio in the vertical mode (ζ_V) was varied from 10% to 40%, and the damping ratio in the fundamental

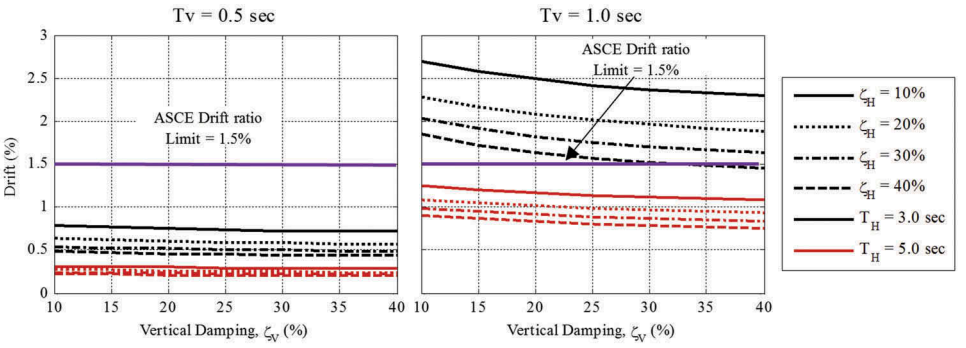

Figure 28. Relative drift ratio between top and bottom of the block for different damping ratios.

horizontal mode (ζ_H) was varied discretely as 10%, 20%, 30% and 40%. Recall that damping in the third (rocking) mode is determined by Rayleigh quotient.

The drift ratio is relatively insensitive to ζ_V when $T_V = 0.5$ s; however, it decreases slightly with increasing ζ_V when $T_V = 1.0$ s. Increasing horizontal damping ratio ζ_H is more effective to reduce the drift than increasing vertical damping, especially for the shorter horizontal isolation period $T_H = 3.0$ s (Fig. 28). Increasing damping up to 40% in both directions ($\zeta_H = 40\%$ and $\zeta_V = 40\%$) is still not sufficient to reduce the drift to the ASCE limit for the combination of $T_H = 3.0$ s and $T_V = 1.0$ s. This implies that the horizontal period T_H should be further lengthened to be paired with T_V as long as 1.0 s. Vertical bearing displacement is more sensitive to ζ_V, and increasing ζ_V is the most effective way to reduce bearing displacement (Fig. 29). $A_{Amp,H}$ has a decreasing trend with increases in both ζ_H and ζ_V; however, the effect is rather minimal for all parameter combinations except $T_H = 3.0$ s and $T_V = 1.0$ s (Fig. 30). Thus, for most reasonable systems, horizontal accelerations cannot be reduced much by increasing the damping. $A_{Amp,V}$ is completely insensitive to ζ_H and can be reduced only slightly by increasing ζ_V (Fig. 31).

Additional analyses are conducted for different combinations of T_H, ζ_H and ζ_V over the range $T_V = 0.5$ to 1.0 s, and the resultant drift ratio and vertical bearing displacement are plotted in Fig. 32. Both drift ratio and bearing vertical displacement are inversely proportional to T_H, ζ_H and ζ_V (meaning that the drift ratio and vertical displacement can be

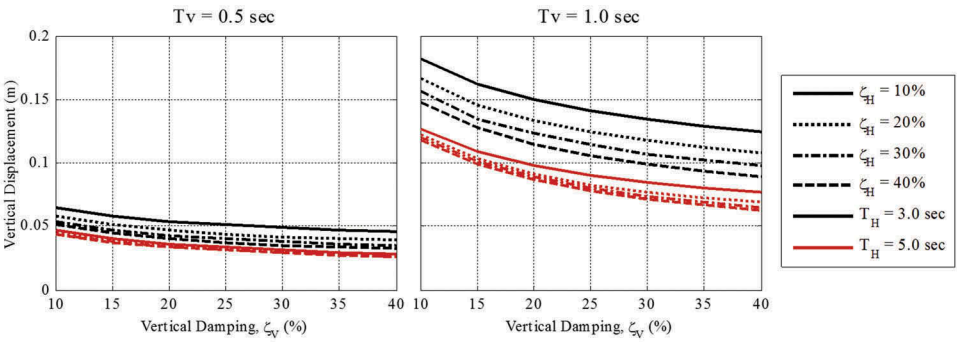

Figure 29. Vertical displacement at left bearing for different damping ratios.

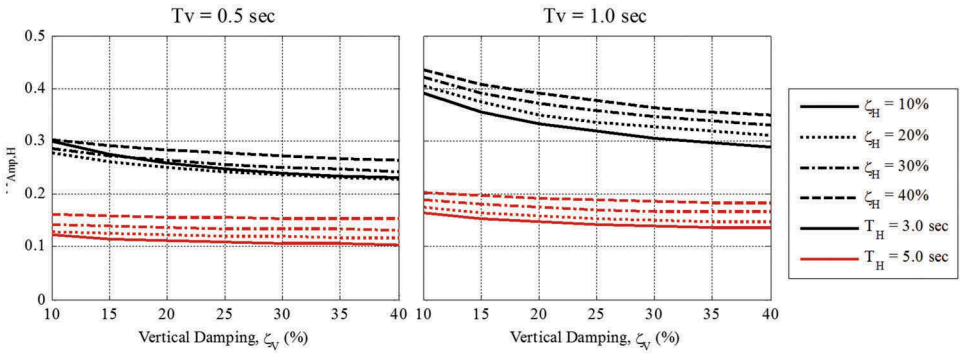

Figure 30. $A_{Amp,H}$ at the block base for different damping ratios.

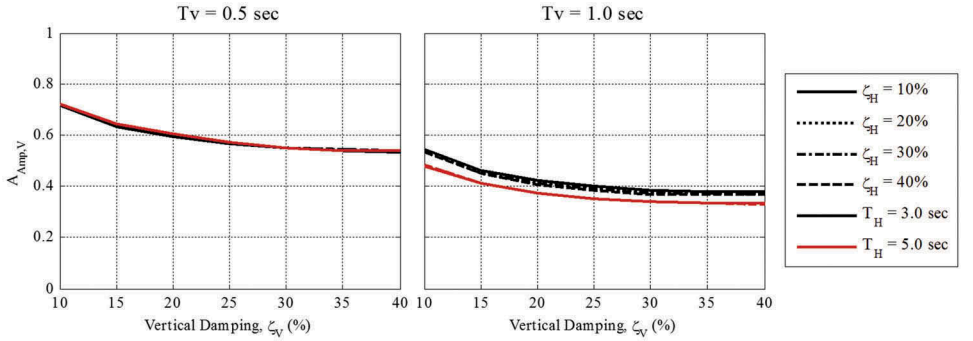

Figure 31. $A_{Amp,V}$ at the block edge different damping ratios.

reduced by increasing any of these parameters). All studied combinations of periods and damping ratios satisfy the ASCE drift ratio limit except moderate horizontal isolation period (T_H = 3.0 s) and baseline damping ($\zeta_H = \zeta_V$ = 20%). In this case, the drift limit can be satisfied by limiting the vertical isolation period T_V < 0.8 s. However, vertical displacement demand is most effectively reduced by decreasing the vertical period as illustrated in Fig. 32.

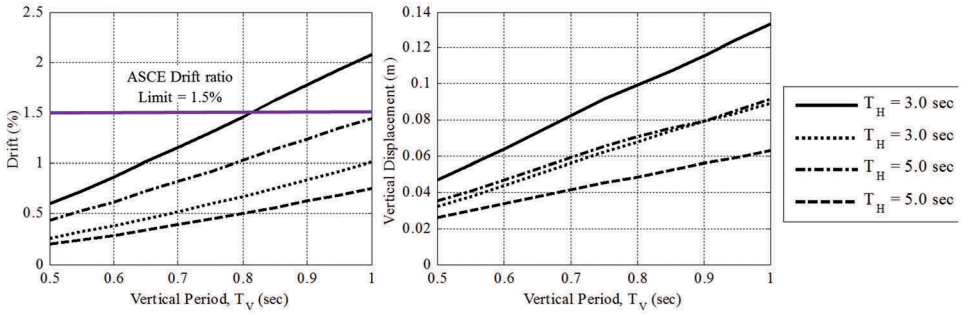

Figure 32. Drift ratio and left bearing vertical displacement for different combinations of T_H, ?$_H$ and ?$_V$.

5.4. *Effect of Superstructure Aspect Ratio*

Recall that all respond trends thus far have been evaluated for a rigid block with aspect ratio $h/b = 2$. Next, the response trends of the rigid block are investigated for different structure aspect ratios (h/b) with various isolation properties. Peak responses are presented as a function of h/b varying from 0.5 to 5, where b is kept constant (9 m) and h varies accordingly. Four isolation system parameter combinations were used in this analysis, $T_H = 3.0$ or 5.0 s, $T_V = 0.5$ or 1.0 s and $\zeta_H = \zeta_V = 20\%$. Median (over the ground motion subset) of the peak values of drift ratio and left bearing vertical displacement for different h/b ratios are presented in Fig. 33. As expected, an increase in aspect ratio increases the rocking effect, which consequently leads to an increase in both drift ratio and vertical bearing displacement (Fig. 33). However, the increase in these responses with aspect ratio is sublinear, which means that the rate of increase slows as aspect ratio. In fact, for some parameter combinations ($T_V = 1.0$ s), the drift ratio and vertical bearing displacement reach a peak for h/b in the range of 2–4 and decrease thereafter.

Both drift ratio and vertical bearing displacement depend strongly on rotation θ, which is influenced by the structure dimension and coupling between horizontal and rocking modes, as illustrated previously. Therefore, modal analysis was carried out for ground motion (#13) to understand the dynamics related to aspect ratio. The modal coordinate q represents the contribution factor of each mode to the total deformation. Response histories of the modal coordinate histories q_1 and q_3, which represent the horizontal and rocking modes, respectively, are presented in Fig. 34 for $T_V = 0.5$ s and Fig. 35 for $T_V = 1.0$ s, while $T_H = 3.0$ s for both. The modal coordinate $q_i(t)$ is multiplied by the mode

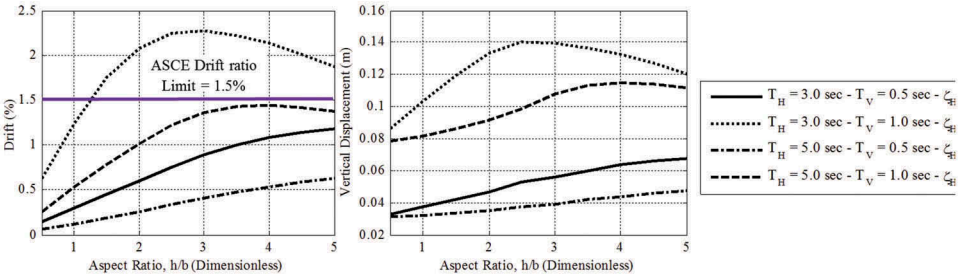

Figure 33. Drift ratio and left bearing vertical displacement for different h/b.

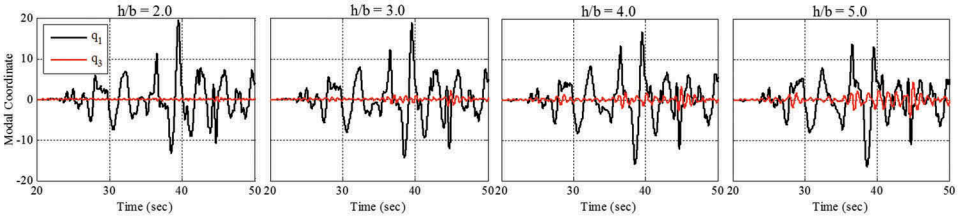

Figure 34. Modal history analysis results at $T_V = 0.5$ s for different h/b.

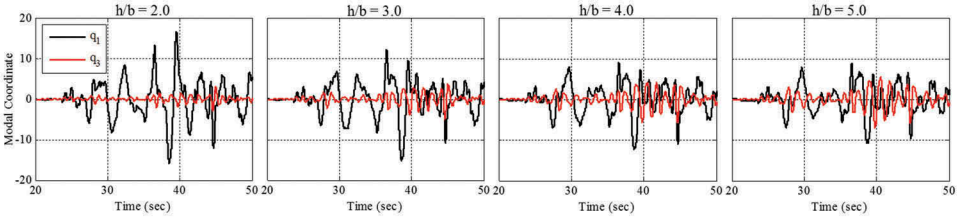

Figure 35. Modal history analysis results at T_V = 1.0 s for different h/b.

shape ϕ_i and summed over all modes to evaluate total displacement and rotation. Note that the mode shapes were normalized such that ${\phi_i}^T m\phi_i = 1$. In general, the modal coordinate q_1 decreases and q_3 increases as h/b increases, which is due to increased coupling between the horizontal mode and rocking mode. For T_V = 0.5, the changes in intensity of the modal coordinates are relatively small, and both drift ratio and vertical bearing displacement increase as h/b increases. However, for T_V = 1.0 s, q_1 decreases and q_3 increases significantly, and q_1 and q_3 are out of phase; consequently, the drift ratio and vertical bearing displacement decrease at $h/b > 3.0$. Increasing aspect ratios do not appear to be a concern for escalating growth in the rocking response; however, for any aspect ratio selecting a shorter T_V will help limit the vertical displacement demand.

5.5. *Effect of Bilinear Stiffness*

If the design ground motion is exceeded, rocking of a building with 3D isolation may cause bearing vertical displacement demands large enough to induce tension in the isolation devices. This is associated with an overturning concern when one side of the building engages in uplift. The authors hereby propose the concept of increasing the isolator resistance to tension relative to compression as an added safeguard against overturning. This can be achieved by designing a vertical or 3D isolator to have bilinear stiffness, with a tension stiffness K_T that differs from the compression stiffness. The objective of a bilinear stiffness is to constrain the peak tensile displacement to very small values – an indication that activating the tension stiffness has arrested the overturning and prevented large tensile displacement demands – while simultaneously attenuating the vertical acceleration.

Additional analyses were conducted to investigate the effectiveness of the proposed concept for controlling or reducing the rocking behavior. The system parameters were selected as follows: rigid block aspect ratio h/b = 2, isolation properties T_H = 3.0 s and T_V = 0.5 s, ζ_H = 20% and ζ_V = 40%. The static displacement of the rigid block due to self-weight or gravity loading is 0.06 m, while the median bearing vertical displacement demand for this system (which can be qualitatively deduced from Fig. 29) is 0.05 m. To evaluate the response when the bearings are consistently subjected to tension, the ground motion subset was scaled up by a factor of 2.0. Median peak values of left bearing vertical displacement and $A_{Amp,V}$ for varying tension stiffness are presented in Fig. 36. The tension stiffness (K_T) is given as a multiple of the compression stiffness (K). The compression displacement is almost independent of K_T; however, tensile displacement slightly decreases as K_T increases, suggesting that the

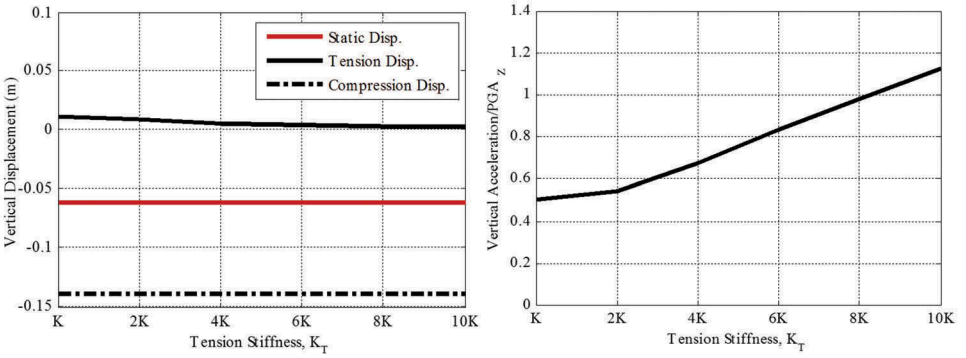

Figure 36. Vertical displacement at left bearing and $A_{Amp,V}$ at block edge for different tension stiffness.

strategy is moderately effective. The vertical acceleration amplification $A_{Amp,V}$ increases with increasing K_T, but vertical acceleration attenuation can be achieved by keeping K_T below $8K$.

6. Conclusion

A simplified rigid block model supported on isolation bearings at the block edges, and subjected to horizontal and vertical ground motion input, was used to investigate the fundamental dynamic response trends of a structure with a 3D isolation system. Furthermore, a multistory frame model was developed to validate the numerical simplified rigid block model. Finally, a parametric study was carried out to evaluate the effect of different site conditions, structure properties and 3D isolation parameters on the structural and isolator responses. This study has led to the following conclusions:

- The rigid block model was shown to be a good simplified model to explore the fundamental dynamic behavior of a 3D isolated structure subjected to horizontal and vertical ground motion excitations. However, the rigid block model does not account for variation in superstructure stiffness and should be used with caution to represent flexible superstructures.
- The rotation θ in rigid block model is shown to be an effective "first-order" prediction of the drift.
- The coupling between horizontal translation and rotation of the rigid block increases with increasing vertical isolation period T_V, which leads to increasing rotation and an associated increase in horizontal displacement at the top of the block (roof level) and a decrease at the base of the block (bearing level).
- Large drifts result even at low values of horizontal period T_H when vertical flexibility is introduced (T_V = 0.5, 1 or 2 s). The drift ratio and bearing vertical displacement are almost constant up to $T_H = T_V$. However, both responses decrease when T_H increases beyond T_V. This suggests that for effective design, T_H and T_V should not be closely coupled, and T_H should be selected to be much longer than T_V.
- The key isolator and structural response parameter trends are not much affected by V/H ratio; rather, governing system parameters are much more influential. Although

the obtained results may be an artifact of the applied ground motions during the analysis, which had similar scale factors when scaled to fit the target spectra with different V/H. However, the chosen ground motions all have large vertical intensity relative to the horizontal.

- Structural responses are seen to increase for increasing site class (increasingly softer soil) over the entire parameter range. The increase in response in site class E compared to D is most pronounced, likely due to significant lengthening of the constant acceleration region of the horizontal spectrum (and corresponding lengthening of the "step" region of the vertical spectrum).
- Increasing horizontal and vertical damping ratios ζ_H and ζ_V leads to decreasing drift ratios and vertical bearing displacement. Increasing the damping ratios is more effective in limiting the drift and bearing displacement demands when T_V = 1.0 s than when T_V = 0.5 s. However, both horizontal and vertical acceleration amplification factors decrease with increasing ζ_V.
- Increasing h/b leads to an increase in rocking, which consequently affects the relative drift ratio between the top and the base and the vertical bearing displacement. However, for T_V = 1.0 s, the drift ratio and vertical bearing displacement decrease at $h/b > 3.0$ due to increased coupling between the horizontal mode and rocking mode as well as those modes becoming out of phase. Although increasing aspect ratios do not appear to be a concern for escalating growth in the rocking response, selecting shorter T_V will help limit the vertical displacement demand for any aspect ratio.
- Based on the results presented in this study, the acceptable range of 3D isolation periods is concluded to be T_V = 0.5 s and $T_H \geq 1.5$ s or T_V = 1.0 s and $T_H \geq 4.0$ s and ζ_H and $\zeta_V \geq 20\%$. These ranges have been selected (a) to keep drift ratio below ASCE limit [ASCE, 2016], (b) to attenuate both horizontal and vertical accelerations and (c) to achieve good separation of horizontal and vertical isolation periods so as to minimize rocking.

Funding

This work was supported by the National Science Foundation (NSF) [CMMI 1437003].

References

Alhan, C. and Gavin, H. P. [2005] "Reliability of base isolation for the protection of critical equipment from earthquake hazards," *Engineering Structures* **27**, 1435–1449. doi:10.1016/j.engstruct.2005.04.007.

American Society of Civil Engineers (ASCE). [2016] *ASCE Standard – ASCE/SEI 7–16: Minimum Design Loads for Buildings and Other Structures*, Reston, VA., American Society of Civil Engineers (ASCE).

Castaldo, P., Palazzo, B. and Della Vecchia, P. [2016] "Life-cycle cost and seismic reliability analysis of 3D systems equipped with FPS for different isolation degrees," *Engineering Structures* **125**, 349–363. doi:10.1016/j.engstruct.2016.06.056.

Chen, J., Liu, W., Peng, Y. and Li, J. [2007] "Stochastic seismic response and reliability analysis of base-isolated structures," *Journal of Earthquake Engineering* **11**, 903–924. doi:10.1080/13632460701242757.

Chiou, B., Daragh, R., Gregor, N. and Silva, W. [2008] "NGA project strong-motion database," *Earthquake Spectra* **24**(1), 23–44. doi:10.1193/1.2894831.

Cutfield, M., Ryan, K. and Ma, Q. [2016] "Comparative life cycle analysis of conventional and base-isolated buildings," *Earthquake Spectra* **32**(1), 323–343. doi:10.1193/032414EQS040M.

Eltahawy, W., Ryan, K., Cesmeci, S. and Gordaninejad, F. [2017] "Fundamental Dynamics of 3-Dimensional Seismic Isolation," *Proceedings of 16th World Conference on Earthquake*, Santiago, Chile.

Furukawa, S., Sato, E., Shi, Y., Becker, T. and Nakashima, M. [2013] "Full-scale shaking table test of a base-isolated medical facility subjected to vertical motions," *Earthquake Engineering and Structural Dynamics* **42**(13), 1931–1949. doi:10.1002/eqe.2305.

Inoue, K., Fushimi, M., Moro, S., Morishita, M., Kitamura, S. and Fujita, T. [2004] "Development of three-dimensional seismic isolation system for next generation nuclear power plant," *Proceedings of 13th World Conference on Earthquake*, Vancouver, B.C., Canada.

Kageyama, M., Iba, T., Umeki, K., Somaki, T., Hino, Y., Moro, S. and Ikutama, S. [2004] "Study on three-dimensional seismic isolation system for next generation nuclear power plant: independent cable reinforced rolling-seal air spring," *Proceedings of 13th World Conference on Earthquake Engineering*, Vancouver, B.C., Canada.

Kageyama, M., Iba, T., Umeki, K., Somaki, T. and Moro, S. [2003] "Development of three-dimensional base isolation system with cable reinforcing air spring," *Proceedings of the 17th International Conference on Structural Mechanics in Reactor Technology*, Prague, Czech Republic.

Kashiwazaki, A., Shimada, T., Fujiwaka, T. and Moro, S. [2003] "Study on 3-dimensional base isolation system applying to new type power plant reactor (hydraulic 3-dimensional base isolation system: No.1)," *Proceedings of the 17th International Conference on Structural Mechanics in Reactor Technology*, Prague, Czech Republic.

Li, X., Xue, S. and Cai, Y. [2013] "Three-dimensional seismic isolation bearing and its application in long span hangars," *Earthquake Engineering and Engineering Vibration* **12**(1), 55–65. doi:10.1007/s11803-013-0151-7.

National Earthquake Hazards Reduction Program (NEHRP). [2009] *Recommended Seismic Provisions for New Buildings and Other Structures. FEMA P-750*, National Earthquake Hazards Reduction Program (NEHRP). Building Seismic Safety Council, A council of the National Institute of Building Sciences, Washington, D.C.

Ryan, K. L., Soroushian, S., Maragakis, E., Sato, E., Sasaki, T. and Okazaki, T. [2016] "Seismic simulation of an integrated ceiling-partition wall-piping system at E-Defense. I: three-dimensional structural response and base isolation," *Journal of Structural Engineering* **142**(2), doi:10.1061/(ASCE)ST.1943-541X.0001384.

Suhara, J., Matsumoto, R., Oguri, S., Okada, Y., Inoue, K. and Takahashi, K. [2005] "Research on 3-D base isolation system applied to new power reactor 3-D seismic isolation device with rolling seal type air spring: Part 2," *Proceedings of 18th International Conference on Structural Mechanics in Reactor Technology*, Beijing, China.

Suhara, J., Matsumoto, R., Torita, H., Tsuyuki, Y., Kamei, T., Takahashi, O., Kunimatsu, Y., Aida, H. and Fujita, T. [2008] "Construction of civil building using three dimensional seismic isolation system: part 2, tests for three dimensional seismic isolation system," *Proceedings of 14th World Conference on Earthquake Engineering*, Beijing, China.

Suhara, J., Tamura, T., Ohta, K., Okada, Y. and Moro, S. [2003] "Research on 3-D base isolation system applied to new power reactor 3-D seismic isolation device with rolling seal type air spring: part 1," *Proceedings of the 17th International Conference on Structural Mechanics in Reactor Technology (SMiRT 17)*, Prague, Czech Republic.

Takahashi, O., Aida, H., Suhara, J., Matsumoto, R., Tsuyuki, Y. and Fujita, T. [2008] "Construction of civil building using three dimensional seismic isolation system: Part 1, Design of building using three dimensional seismic isolation system," *Proceedings of 14th World Conference on Earthquake Engineering*, Beijing, China.

Terzic, V., Mahin, S. A. and Comerio, M. C. [2014] "Comparative life-cycle cost and performance analysis of structural systems," *Proceedings of the 10th National Conference in Earthquake Engineering, Earthquake Engineering Research Institute*, Anchorage, AK.

Terzic, V. A. and Mahin, S. A. [2017] "Using PBEE to access and improve performance of different structural systems for low-rise steel buildings," *International Journal of Safety and Security Engineering* **7**(4), 532–544. doi:10.2495/SAFE-V7-N4-532-544.

Xu, Z. D., Huang, X. H. and Lu, L. H. [2012a] "Experimental study on horizontal performance of multi-dimensional earthquake isolation and mitigation devices for long-span reticulated structures," *Journal of Vibration and Control* **18**(7), 941–952. doi:10.1177/1077546311418868.

Xu, Z. D., Tu, Q. and Guo, Y. F. [2012b] "Experimental study on vertical performance of multi-dimensional earthquake isolation and mitigation devices for long-span reticulated structures," *Journal of Vibration and Control* **18**(13), 1971–1985. doi:10.1177/1077546311429338.

Zhou, Z., Wong, J. and Mahin, S. [2016] "Potentiality of using vertical and three-dimensional isolation systems in nuclear structures," *Nuclear Engineering and Technology*, doi:10.1016/j.net.2016.03.005.